PCCP

Accepted Manuscript

This article can be cited before page numbers have been issued, to do this please use: Y. Zhou, S. Ayad, C. Ruchlin, V. Posey, S. P. Hill, Q. Wu and K. Hanson, *Phys. Chem. Chem. Phys.*, 2018, DOI: 10.1039/C8CP03628D.

View Article Online
DOI: 10.1039/C8CP03628D

Examining the Role of Acceptor Molecule Structure in Self-Assembled Bilayers: Surface Loading, Stability, Energy Transfer, and Upconverted Emission

lReceived 00th January 20xx,
Accepted 00th January 20xx

DOI: 10.1039/x0xx00000x

www.rsc.org/

Yan Zhou[a], Suliman Ayad[a], Cory Ruchlin[a], Victoria Posey[a], Sean P. Hill[a], Qiang Wu[b], and Kenneth Hanson[a]*

Self-assembly of sensitizer and acceptor molecules has recently emerged as a promising strategy to facilitate and harness photon upconversion *via* triplet-triplet annihilation (TTA-UC). In addition to the energetic requirements, the structure and relative orientation of these molecules can have a strong influence on TTA-UC rates and efficiency. Here we report the synthesis of five different acceptor molecules composed of an anthracene core functionalized with 9,10- or 2,6- phenyl, methyl, or directly bound phosphonic acid groups and their incorporation into self-assembled bilayers on a ZrO_2 surface. All five films facilitate green-to-blue photon upconversion with Φ_{uc} as high as 0.0023. The efficiency of TTA, and not triplet energy transfer, fluorescence, or losses via FRET, was primarily responsible for dictating the Φ_{uc} emission. Even for molecules having similar photophysical properties, variation in the position of the phosphonic acid resulted in dramatically different Φ_{TTA}, I_{th} values, γ_{TTA}, and D. Interestingly, we observed a strong linear correlation between Φ_{TTA} and the I_{th} value but the cause of this relationship, if any, is unclear.

1. Introduction

Photon Upconversion via triplet- triplet annihilation (TTA-UC), wherein two low energy photons are combined to generate higher energy excited state, is of interest for a number of applications including bioimaging,[1, 2] oxygen sensing,[2] photocatalysis,[3] and solar energy conversion.[4-11] Regarding the latter, TTA-UC is particularly intriguing since it provides a means of surpassing the Shockly-Queisser limit (~33%)[12] and increase maximum theoretical solar cell efficiencies to upwards of 43% under AM 1.5 solar irradiation.[9,13,14]

During TTA-UC, a sensitizer molecule (**S**) absorbs a low energy photon, then undergoes intersystem crossing followed by triplet energy transfer to an acceptor (a.k.a an annihilator or emitter) molecule (**A**). When two **A** triplet excited states are in proximity they can undergo TTA where emission from the resulting singlet excited state is hypsochromically shifted relative to the excitation light and thus the photon energy is upconverted during the process.

A majority of TTA-UC research has been performed with sensitizer and accepter molecules suspended in solution or a rubbery polymer matrix.[15-21] Through this effort, a great deal has been learned about how the thermodynamics of the molecules suspended in a medium can influence TTA-UC. For example, subtle variations in the structure of the prototypical anthracene acceptor molecule[22] can have a large impact on the triplet excited state lifetime, singlet/triplet potential energy surface, and ultimately the TTA-UC yield.[23-25]

Building upon these host-based UC schemes, recently there has been a sharp increase in using supramolecular assemblies[26, 27] like micelles/lipid membranes,[28] polymers/dendrimers,[29, 30] host-guest interactions,[31] ionic crystals,[32] and MOFs[33, 34] to facilitate TTA-UC. Of the assembly strategies, binding **S** and **A** molecules on nanocrystalline metal oxide surfaces (TiO_2 or ZrO_2) has emerged as a means of not only facilitating UC emission,[10, 35-38] but also extracting charge from the upconverted state and directly harnessing TTA-UC in a solar cell.[5, 6, 10, 33, 39, 40] Self-assembled bilayers (Figure 1a) are particularly promising in that under solar flux, TTA-UC photocurrents of >0.1 mA/cm^2 have been achieved which is above the device relevance threshold proposed by Schmidt and coworkers.[41]

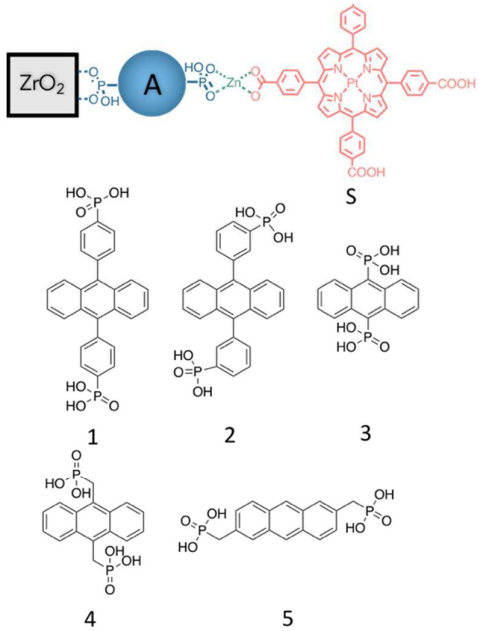

[a] Department of Chemistry & Biochemistry, Florida State University, Tallahassee, Florida 32306, United States
[b] National High Magnetic Field Laboratory, High-Performance Materials Institute, Tallahassee, Florida 32310, United States
Electronic Supplementary Information (ESI) available: See DOI: 10.1039/x0xx00000x

View Article Online
DOI: 10.1039/C8CP03628D

Figure 1 . Schematic representation of the self-assembled bilayer on ZrO_2 and structures for Pt(II)-tetrakis(4-carboxyphenyl)porphyrin (**S**) and acceptor molecules (**1**-**5**).

The bilayer films are prepared by stepwise soaking[42] of a metal oxide film in an a solution of **A**, then linking metal ion, and finally **S**.[39] Unlike in a solvent or host matrix, where molecules are relatively free to rotate and collide, these assembled systems geometrically restrict the mobility and orientation of the **S** and **A** molecules. Thus, in addition to the energetic influence noted above, presumably structural variations that tune intermolecular distance and orientation are critical in dictating TTA-UC rates and efficiencies.

Recently, our group reported that for two energetically similar diphenylanthracene molecules (**1** and **2** in Fig 1), changing the phosphonate metal ion binding group from the *para*- to the *meta*- position results in a 3-fold decrease in the TTA-UC emission quantum yield.[11] In an effort to further elucidate the role of the acceptor structure on TTA-UC in bilayer films, here we report the synthesis of three new anthracene dyes substituted at the 9,10- or 2,6- positions with phosphonate metal ion binding groups (Figure 1). The photophysical properties of the dyes **1**-**5** in solution, on films and combined with Pt(II)- tetrakis(4-carboxyphenyl)porphyrin (**S**) sensitizer in the bilayer film are described.

2. Experimental section

2.1 Materials.

1,4-Dibromobenzene, 1,3-Dibromobenzene, anthraquinone, n-butyl lithium, nickel bromide, triethylphosphite, trimethylsilyl bromide, toluene, benzene, benzyl alcohol, N,N-dimethylformamide, aluminium chloride, chromium(VI) oxide, copper(II) sulfate, zinc powder, potassium carbonate, N-bromosuccinimide, 9,10-dibromoanthracene, acetic anhydride, 95% sulfuric acid, glacial acetic acid, hydrochloric acid, ammonium hydroxide solution, bis(dichloromethyl)anthracene, iodomethane, 2,3-dichloro-5,6-dicyano-1,4-benzoquinone, phosphorus tribromide, lithium aluminium hydride, zinc acetate dihydrate, and Pt(II) meso-tetra(4-carboxyphenyl)porphine (Frontier Scientific), were purchased from their respective suppliers, in parentheses, and used as received.

All other reagents and solvents (analytical reagent grade) have been purchased and used without further purification from Alfa Aesar. Tetrahydrofuran and dichloro-methane used in synthesis have been dried and degassed prior to use. Glass substrate was purchased from Hartford Glass Co. Meltonix film (1170–25) and Vac'n Fill Syringe (65209) were purchased from Solaronix. Micro glass cover slides (18 × 18 mm) were obtained from VWR. ZrO_2 sol gel paste and nanocrystalline films were prepared following previously reported procedures was prepared following a previously reported procedure.[43-45]

2.2 Sample preparation-device fabrication

Spectroscopic samples were prepared in a sandwich cell-type architecture.[5, 6, 11, 39, 40, 46] Briefly, glass was cut into 2.2 × 2.2 cm pieces, and an active area of 1 cm^2 metal oxide was prepared by doctor blading ZrO_2 (1 layer of Scotch tape) and sintering. Dyes were then loaded onto the metal oxide, as described below. A small hole (d = 1.1 mm) was drilled into the corner of the 2.2 × 2.2 cm glass slide. A 2 mm wide 2.2 × 2.2 cm Meltonix film was placed between the two glass slides, and the entire ensemble was heated to ~150 °C for 7 s using a home-built heating/sealing apparatus described previously.[47] The cells were then transferred to a glovebox (VTI Universal Purified Glovebox, N2 atmosphere) where dry and oxygen-free acetonitrile was injected using a Vac'n Fill Syringe through the 1 mm hole to fill the interior of the cells. A meltonix film and small piece of micro glass cover slide were then heated to seal the hole used for solvent injection.

2.3 Sample preparation-film formation

Photophysical cells were prepared following our previously published procedure with minor modification.[5, 6, 11, 39, 40, 46] Adsorption isotherms of the **A** molecules on ZrO_2 were measured by immersing thin films in 3 mL of DMSO solution of **1**–**5** with concentrations of 25, 50, 70, 100, 200, 300, 400 and 500 μM. The slides were removed, rinsed with methanol, and dried under a stream of air. Greater details will be seen in the results and discussion section.

2.4 Surface area measurement

The surface area of the ZrO_2 nanocrystalline film were determined from nitrogen adsorption-desorption isotherms at 77 K (Quantachrome Corportion, Autosorb iQ.). Surface area were determined using BET equation.[48] The samples were degassed under vacuum (5×10^{-3} mmHg) at 120 °C for 4 h, prior to measurement, to evacuate physiosorbed moisture. Surface area was calculated to be 113.6 m^2/g. 4 strips of 10 cm × 1.5 cm ZrO_2 film were scraped off from the glass and dried on the oven overnight, and yielded 30.1 mg, which further gives us the surface area ($A_{1\times1}$) of 1 cm × 1 cm film area is 565 cm^2.

2.5 Photostability Measurements

The light from a Blue (375 nm, fwhm ~30 nm, 1.53 mW/cm^2) Mounted high power LED (Thorlabs, Inc., M455L2) powered by a T-Cube LED driver (Thorlabs, Inc., LEDD1B). Light output was directed onto the derivatized thin films placed at 45° in a standard 10 mm path length cuvette containing 3 mL of MeCN. The illumination spot was adjusted to coincide both with the thin films and the perpendicular beam path of a Varian Cary 50 UV–vis spectrophotometer. The absorption spectrum (360–800 nm) of the film was obtained every 10 s during 11600s (decreased by 5% after the first 4000s measurement). The incident light intensity was measured

View Article Online
DOI: 10.1039/C8CP03628D

using a thermopile detector (Newport Corp 1918-C meter and 818P-020-12 detector). The solution temperature, 22 ± 2 °C, was consistent throughout the duration of the experiment.

2.6 Absorption measurements

Absorption spectra were recorded on an Agilent 8453 UV-visible photo diode array spectrophotometer. Extinction coefficients for **A**s in DMSO were determined from the absorption spectra of solutions with a known concentration of dye in a 1 × 1 cm quartz cuvette. Thin film absorption spectra were obtained by placing dry, derivatized ZrO2 slides perpendicular to the detection beam path.

2.7 Steady-State Emission

Edinburgh FLS980 fluorescence spectrometer was used to collected emission data at room temperature. A housed 450 W Xe lamp/single grating (1800 λ/mm, 250 nm blaze) Czerny–Turner monochromator or a Nd:YAG laser (Aixiz, AD-532-400T) was used as output to excite the samples. Nd:YAG laser was passed through a variable neutral density filter (Edinburgh F-B01 laser mount), a 2 mm diameter iris (Newport ID-1.0) and then directed to the sample via a flip mirror. Emission from the sample were passed through a 532 nm notch filter (Thorlabs Inc., NF533-17), the single grating (1800 l/mm, 500 nm blaze) Czerny–Turner monochromator and then detected by a Peltier-cooled Hamamatsu R928 photomultiplier tube. A power meter (Ophir Vega 7Z01560) with a high sensitivity power sensor (Ophir 3A-FS 7Z02628) was used to measure laser intensities. Fluorescence quantum yield of **A** in DMSO are estimated relative to DPA in EtOH (Φ_F = 95%)[49] by $\Phi_A = \Phi_{DPA}\frac{I_A A_{DPA} n_A^2}{I_{DPA} A_A n_{DPA}^2}$,[39] where $I_{\mathbf{A}}$ and I_{DPA} are the integrated emission intensities of **A** in DMSO and DPA in EtOH (from 380- 550 nm) under the excitation of 360 nm, respectively. $A_{\mathbf{A}}$ and A_{DPA} are their respective absorbance at 360 nm. 1.36[50] and 1.47[51] are used for the refractive indices of $\eta_{\mathbf{A}}$ and η_{DPA}. Emission quantum yields for upconverted emission from ZrO_2-**A**-Zn-**S** (**A**= **2** ~ **5**) are estimated relative to using equation $\Phi_{UC} = \Phi_{UC1}\frac{I_{UC} A_{UC1} n_{UC}^2}{I_{UC1} A_{UC} n_{UC1}^2}$ Where I_{UC} and I_{UC1} are the integrated emission intensities of ZrO_2-**1**-Zn-**S** and ZrO_2-**A**-Zn-**S**, respectively. A_{UC} and A_{UC1} are their respective absorbance at 532nm. Given the similar cell architecture, composed of glass, ZrO_2 and MeCN, the refractive indices (η_{UC} and η_{UC1}) are assumed to be the same for both samples. The emission intensities were acquired with 532 nm excitation (2.5 W/cm^2) using the sandwich cell architecture placed at an ~45 degree angle relative to the incident excitation. Emission, perpendicular to the incident laser was passed through a 532 nm notch filter (Thorlabs Inc., NF533-17) before entering the monochromator/detector.

2.8 Time-resolved Emission

Emission decay kinetics, not including TTA-UC emission, were collected at room temperature using an Edinburgh FLS980 fluorescence spectrometer. The emission decay traces were acquired using either time-correlated single-photon counting (TCSPC; 1024 channels; 200 ns window) with data collection for 10000 counts or multichannel scaling (MCS) acquisition mode with 532 nm excitation from a 60 W microsecond flashlamp (pulse width <2.5 μs) at a 100 Hz repetition rate for lifetime measurements of **A**s and PtP, respectively. TCSPC excitation was provided by an Edinburgh EPL-360 ps pulsed light emitting diode (360 ± 10 nm, pulse width 892 ps) operated at 10 MHz. Emission was passed through a single grating (1800 l/mm, 500 nm blaze) Czerny– Turner monochromator and detected by a Peltier-cooled Hamamatsu R928 photomultiplier tube. Emission decay kinetics for the films were fitted with a biexponential function $y = A_1e^{-k1x} + A_2e^{-k2x} + y_0$ using the Edinburgh software package, and a weighted average lifetime calculated using $\langle\tau\rangle = \Sigma A_i\tau_i^2/\Sigma A_i\tau$.

TTA-UC emission decays for **A** and **PtP** in DMSO used to determine τ_A^3 were collected using an Edinburgh Instruments LP980-KS laser flash photolysis spectrometer. Measurements were carried out using sealed 1 × 1 cm quartz cuvette containing oxygen free DSMO solutions. The spectrometer is composed of a Continuum Surelite EX Nd:YAG laser combined with a Continuum Horizon OPO (532 nm, 5−7 ns, operated at 1 Hz, beam diameter ~0.5 cm, 2.5−5 mJ/pulse) integrated into the Edinburgh LP980 spectrometer. For time-resolved scans, the emission was passed through a TMS302-A monochromator (1800 grooves/mm grating) with a 300 mm focal length in Czerny Turner configuration and detected Hamamatsu R928 photomultiplier tube. Edinburgh's L900 (version 8.2.3, build 0) software package was used to process detector outputs. As with emission, the decay kinetics were fit using a biexponential function, and the results are presented as a weighted average lifetime.

3. Result and discussion

3.1 Acceptor design and synthesis

Acceptor molecules 4,4-(anthracene-9,10-diyl)bis(4,1-phenylene) diphosphonic acid (**1**),[39] and 4,4'-(anthracene-9,10-diyl)bis(3,1-phenylene)diphosphonic acid (**2**)[11] were prepared by following previously published procedures. Anthracene-9,10-diphosphonic acid (**3**)[52] and anthracene-9,10-diylbis(methylene) diphosphonic acid (**4**)[53] were prepared by first generating the ethyl ester compounds from 9,10-dibromo anthracene and 9,10-bis(dichloromethyl)anthracene, respectively, using variations of the Arbuzov reaction,[54] followed by ester group cleavage using TMS-Br.

The multistep synthesis of 2,6-anthracenediylbis(methylene)bisphosphonic acid (**5**) is shown

View Article Online
DOI: 10.1039/C8CP03628D

Table 1. Photophysical properties of **1**-**5** in DMSO.

	λ_{abs} (nm) (ε, × 10^4 M^{-1} cm^{-1})	λ_{em} (nm)[a]	τ_{S1} (ns)[a,b]	Φ_{FL}[a]	k_r (s^{-1})[d]	k_{nr} (s^{-1})[e]
1	358 (0.77), 376 (1.29), 397(1.22)	419, 433	5.9	0.93	1.6×10^8	1.2×10^7
2	358(0.72), 376 (1.16), 397(1.10)	414, 433	6.1	0.92	1.5×10^8	1.3×10^7
3	371(0.54), 388 (0.68), 410(0.60)	428, 446	10.9	0.79	7.3×10^7	1.9×10^7
4	365(0.64), 385 (1.10), 407(1.09)	413, 436, 462	10.1	0.85	8.4×10^7	1.5×10^7
5	348(0.36), 366 (0.47), 385(0.36)	429, 444, 459	5.2	0.14	2.7×10^7	1.7×10^8

[a]λ_{ex} = 360 nm. [b]From an exponential fit to the excited state decay at the emission maximum. [d]$k_r = \Phi_{FL}/\tau_{S1}$. [e]$k_{nr} = (1-\Phi_{FL})/\tau_{S1}$.

in Scheme 1. Briefly, 2,6-dimethylanthracene (**5a**) was prepared from benzyl alcohol following the procedure of Cao et al.[55] Initially we attempted to generate 2,6-bis(bromomethyl)anthracene (**5d**) using N-bromosuccinimide (NBS) following a previously published procedure.[56] However, bromination of the methyl substituents was unsuccessful presumably due to the higher reactivity of the 9 and 10 positions of the anthracene core.[57, 58] Instead the product was synthesized by oxidizing the methyl groups with CrO_3 (**5b**), followed by reduction and rearomatization of the anthroquinone core, and further reduction to obtain 2,6-bis(hydroxymethyl)anthracene (**5c**). Bromination at the methyl positions was then achieved with PBr_3 (**5d**) followed by an Arbuzov reaction and finally ester group cleavage to yield **5**.

Scheme 1. Synthetic scheme for molecule **5**.

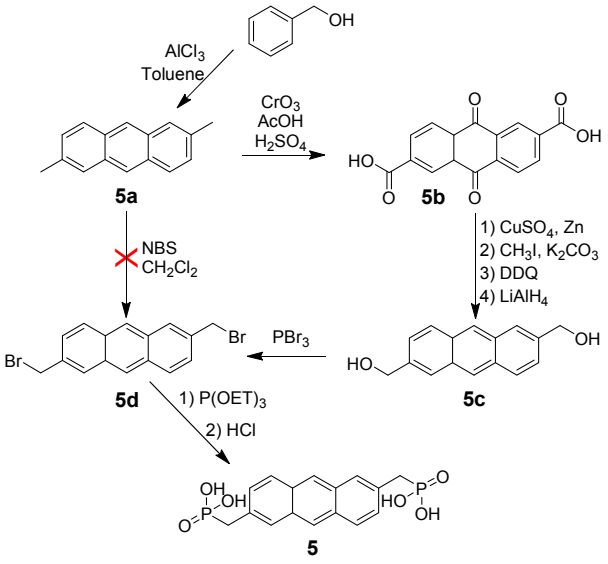

3.2 Solution photophysics

The photophysical properties of **1**-**5** dissolved in DMSO are summarized in Table 1. As can be seen in Figure 2a, the absorption spectral features of **1**-**5** are similar with the characteristic vibronic progression of anthracene.[59] Relative to the parent anthracene (λ_{abs} = 380 nm; Figure S1), the substituted compounds exhibit a bathochromic shift in the order of **5** (λ = 385 nm) < **1** (λ = 398 nm) ≈ **2** (λ = 398 nm) < **4** (λ = 406 nm) < **3** (λ = 410 nm). Similar to that of 9,10-diphenylanthracene, the bathochromic shift in **1** and **2** is due to increased conjugation between anthracene core and the phenyl substituents at the 9,10- positions.[59] As noted previously,[11] absorption energies and extinction coefficients of **1** and **2** are similar indicating that the phosphonate groups are sufficiently decoupled as to not strongly influence the anthracene chromophoric unit. While **4** and **5** are both methylphosphonic acid derivatives, substitution at 9,10-position (**4**) results in a 0.25 eV hypsochromic shift relative to anthracene, whereas 2,6- substitution (**5**) has a nominal effect on the absorption energy but lowers the extinction coefficient. Similar spectral shift has been observed by Jones et al. for dimethylanthracene where this behavior is attributed to greater π electron delocalization at the 9,10- position relative to the 2,6- position.[59] Compound **3** exhibits the largest hypsochromic shift presumably due to the electron withdrawing PO_3H_2 groups being bound directly to the anthracene core. The trend in emission energies for **1**-**5** (Fig 2b) is comparable to that observed for their absorption. However, while the quantum yield (Φ_{FL} > 0.80) as well as radiative ($k_r \approx 1 \times 10^8$ s^{-1}) and non-radiative ($k_{nr} \approx 1 \times 10^7$ s^{-1}) rates are similar for **1**-**4**, there is a notable decrease in emission quantum yield for **5** (Φ_{FL} = 0.14) which is due to the four-fold decrease in k_r (2.4×10^7 s^{-1}) and an order of magnitude increase in k_{nr} (1.5×10^8 s^{-1}).

3.3 ZrO_2-A film formation, photophysics, and photostability

The bilayer films were prepared using a step-wise soaking procedure first implemented by Mallouk, Haga, and others on planar surfaces [45, 60, 61] and then later extended to mesoporous substrates.[42] Briefly, nanocrystalline ZrO_2 is first soaked in a DMSO solution of **A** for 12 hours, then Zn^{II}, and finally a DMSO solution of **S**.[39] Each step of the surface modification procedure was monitored by UV–Vis or attenuated total reflectance infrared (ATR-IR) spectroscopy. ZrO_2 was chosen as the substrate for this work because its relatively high conduction band potential which inhibits excited state electron transfer from the dyes to the metal oxide surface and thus emission can be observed without concerns of quenching by the substrate.[62,63]

The binding of **1**-**5** to ZrO_2 obeys Langmuir isotherm behavior[64] with the maximum surface coverage (Γ_{max}) and the surface adsorption constant (K_{ad}) reported in Table 2. Surface

View Article Online
DOI: 10.1039/C8CP03628D

Table 2. Surface loading and photophysical properties of ZrO_2-**A**.

	Γ_{max} (mol/cm^2) [a]	d_{A-A} (Å)[b]	λ_{abs} (nm)[c]	λ_{em} (nm)[d]	τ_{S1} (ns)[d,e]	K_{ad} (mmol^{-1})[f]	τ_{dec} (s)[g]	k_{dec} (s^{-1})[h]
1	1.0×10^{-7}	8.6	360, 378, 399	458	7.6	0.016	420	0.0027
2	9.8×10^{-8}	9.7	360, 378, 398	447	6.6	0.012	400	0.0026
3	7.8×10^{-8}	16.0	391, 412	466	2.6	0.019	1000	0.0011
4	9.6×10^{-8}	11.2	365, 383, 403	471	6.8	0.020	310	0.0032
5	9.9×10^{-8}	8.9	346, 364, 383	464	11.1	0.018	290	0.0044

[a] Calculated using $\Gamma = (A(\lambda)/\varepsilon(\lambda))/1000$. [b] Calculated from the ZrO_2 surface area and total dye loading. [c] Measured in DMSO. [d] λ_{ex} = 360 nm. [e] Weighted average lifetime from the biexponential fit. [f] Calculated using Langmuir equation: $(\Gamma = \Gamma_{max}((K_{ad}[A])/(1+ K_{ad}[A])))$. [g] Weighted average lifetime from the biexponential fit of Figure 4b. [h] $k_{dec} = \tau_{dec}^{-1}$.

coverages (Γ in mol/cm^2) are estimated with the expression $\Gamma = (A(\lambda)/\varepsilon(\lambda))/1000$, where $A(\lambda)$ is the maximum absorbance of each molecules on the slides and ε is the molecular molar extinction coefficient for the dyes in DMSO.[65] From the isotherms(Figure S2) , it was determined that a 250 μM of **1** and a 300 μM solutions of **2**-**5** were sufficient to achieve high surface loadings (~1 × 10^{-8} mol/cm^2) and was used for all measurementsreported below.

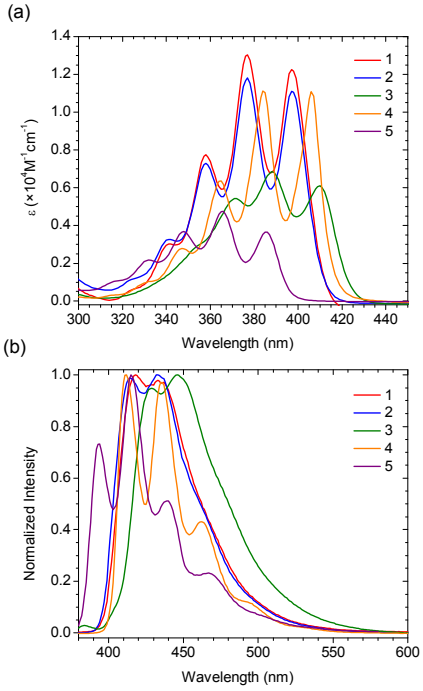

Figure 2. Absorption (a) and emission (b) spectra for **1-5** in DMSO (λ_{ex} = 360 nm).

Because the Γ_{max} values are only a relative estimate of surface coverage and are film thickness dependent, we sought out to determine the center-to-center distance between **A** molecules (d_{A-A}) and the results are summarized in Table 2. These values were determined by first quantifying the surface area of ZrO_2 using BET isotherm measurements with N_2 as the adsorbent. The dye molecules were then loaded on the surface under full coverage conditions, desorbed by soaking the films in a 0.1 M KOH solution, and the amount of loaded dye was calculated from the absorption intensity of the solution using Beer's law (see supporting information for more details). The d_{A-A} values were then calculated from the surface area and total number of dye molecules assuming hexagonal packing of spherical molecules. The d_{A-A} for **1**, **2**, **4**, and **5** were similar ranging from 9-11 Å. Compound **3** exhibited the largest intermolecular spacing at 16 Å. Given the similarity in size of these molecules it is not entirely clear to us why **3** would exhibit a lower surface coverage and larger intermolecular distance. Regardless, all intermolecular spacing are sufficiently close such that intermolecular Dexter energy transfer[66] and TTA can occur.[67, 68]

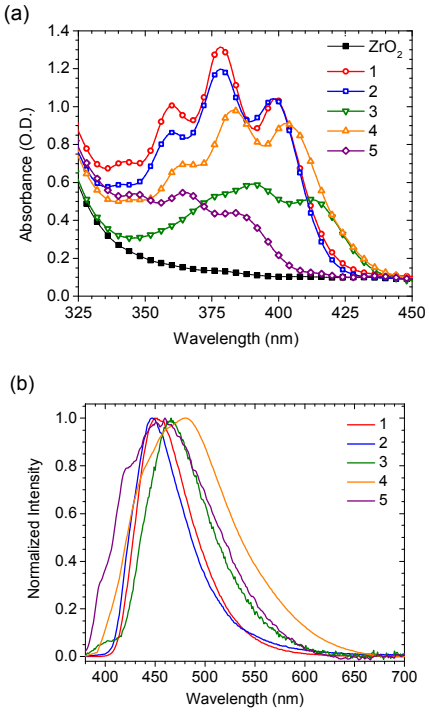

Figure 3. (a) Absorption spectra in air and (b) emission spectra in acetonitrile for **1**-**5** on ZrO_2. (λ_{ex} = 360 nm)

View Article Online
DOI: 10.1039/C8CP03628D

The absorption and emission spectra for **1**-**5** bound to ZrO_2 (here in referred to as ZrO_2-**A**) are shown in Figure 3a and 3b, respectively. The dyes on ZrO_2 exhibit similar absorption energies and spectral features as in solution (Figure 3a). Upon excitation at 360 nm, blue emission is observed from all ZrO_2-**A** films (Figure 3b) with similar but broadened emission features when compared to in solution.

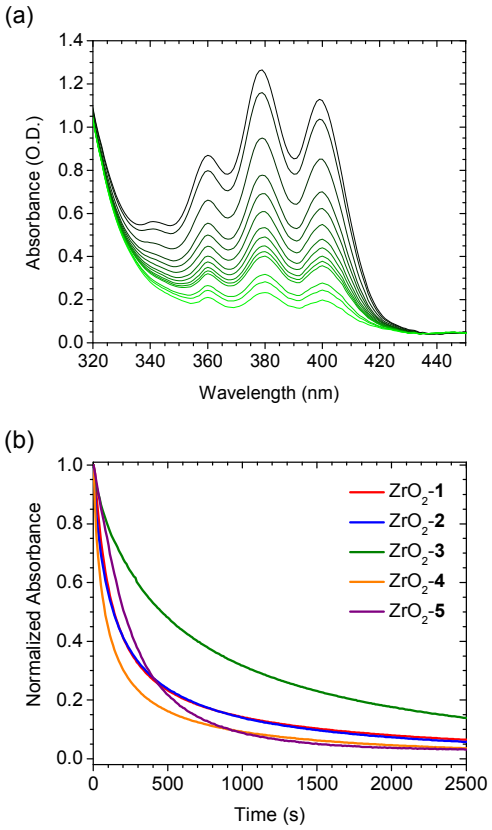

Figure 4. Changes in the absorption spectrum of a) ZrO_2-**1** in MeCN under constant 365 nm (1.5 mW/cm^2) irradiation from 0 (black) to 2 hours (green) and b) the normalized absorbance intensity versus time for **1**-**5** on ZrO_2 in MeCN.

The photostability of acceptor molecules is critical to maintaining high TTA-UC efficiencies for long term applications. This is a particular concern with anthracene molecules since they are known to undergo dimerization and decomposition.[69, 70] With this in mind, the photostability of ZrO_2-**A** films in MeCN were investigated following previously published procedure[71] by monitoring changes in the absorbance spectrum of the films under continuous 365 nm irradiation (1.5 mW/cm^2). The results for ZrO_2-**1** can be seen in Figure 4a with the remaining spectra in the supporting information. For the films of **1**-**5** there is a uniform decrease in absorption intensity at all wavelengths. There was no absorption from the external solution after irradiation and color did not return after heating the films to 80 °C overnight indicating that that the spectral changes are due to dye decomposition and not desorption or photo-dimerization of **A**.[69] Under similar conditions but using deaerated MeCN, the decomposition is slowed by several orders of magnitude (Figure S4). Given their sensitivity to atmosphere, the photoinduced dye decomposition is presumably due to the well known [4+2] cyclcoaddition of singlet oxygen across the 9,10-positions of anthracene.[70]

The time-dependent changes in absorption were fit with the biexponential function and are presented as an average decomposition rate constant (k_{dec}) calculated as the inverse of the weighted-average lifetime ($k_{dec} = \langle\tau\rangle^{-1}$), and the results are summarized in Table 2. The spectral change and desorption rate constant was reproducible within ±10 % across two independently prepared samples.

Of the films, ZrO_2-**4** and ZrO_2-**5** were the least stable decomposing with a rate constant greater than 3×10^3 s^{-1}. Slightly more stable ($k_{dec} = 2.6 \times 10^3$ s^{-1}) were diphenyl substituted compound **1** and **2**. The phenyl substituents are known to decrease reactivity at the 9,10- positions due to increased steric hindrance.[72] Interestingly, compound **3** was the most stable of the series which may be due to similar steric hinderance and/or a change in reactivity at the 9,10 position due to the phosphonate groups.

3.4 ZrO_2-A-Zn-S film formation

Zn^{II} was chosen as the metal linking ion for bilayer film formation because it is photophysically and electrochemically inert under the measurement conditions applied here.[73] Zn^{II} coordination to the non-surface bound phosphonate groups of **A** was achieved by soaking the ZrO_2-**A** films in a solution of 400 μM $Zn(CH_3COO)_2$ in methanol for 30 minutes.[5, 39, 40, 46] Metal ion coordination was monitored using ATR-IR spectroscopy and the results shown in supporting information. All ZrO_2-**A** films exhibit a peak at ~950 cm^{-1} that is indicative of O-P-O bending of the non-surface bound PO_3H_2 group.[74] Upon soaking ZrO_2-**A**, the ~950 cm^{-1} peak disappears with concomitant growths of features at 1000 to 1150 cm^{-1} consistent with metal ion coordination to the PO_3H_2 groups of **1**-**5**.[75]

The bilayer film (ZrO_2-**A**-Zn-**S**) was then prepared by submerging ZrO_2-**A**-Zn in a 100 μM solution of **S** in DMSO. The soaking time for each film (see SI for treatment times) was varied to generate films with an **A** to **S** ratio of 10 to 1 which was previously reported to minimize "self-filtering" losses and maximize TTA-UC emission from bilayer films.[39] Upon soaking ZrO_2-**A** in a solution of **S**, without a $Zn(CH_3COO)_2$ treatment, there was minimal absorption contribution from the porphyrin molecule (Figure S6). This observation indicates that the surface coverage of **A** is sufficiently high to inhibit the sensitizer from binding directly to the ZrO_2 surface.

While we do not have direct structural information about the interface, the necessity of Zn^{II} linking ions for **S** loading supports the formation of a bilayer architecture similar to that depicted in Figure 1 and not a co- deposited film. The

View Article Online
DOI: 10.1039/C8CP03628D

lack of structural data also brings into question the dynamic motion of the molecules on the surface which would influence the energy transfer and TTA dynamics. Previously published

Table 3. Quantum yields for the TTA-UC processes of ZrO_2-**A**-Zn-**S** in oxygen free MeCN (**A** = **1**-**5**).

A	Φ_{uc} [a]	Φ_{FL}	k_{TET} (s^{-1}) [b]	Φ_{TET} [c]	J (cm^3M^{-1}) [d]	k_{FRET} (s^{-1}) [e]	Φ_{FRET} [f]	Φ_{out} [g]	Φ_{TTA} [h]
1	0.0023	0.93	1.3×10^4	0.33	2.6×10^{-11}	7.75×10^6	0.05	0.95	0.0057
2	0.0008	0.92	1.3×10^4	0.33	2.8×10^{-11}	9.30×10^6	0.06	0.94	0.0020
3	0.0004	0.79	2.1×10^4	0.59	3.3×10^{-11}	2.44×10^8	0.38	0.62	0.0009
4	0.0007	0.85	1.7×10^4	0.52	3.4×10^{-11}	2.37×10^7	0.14	0.86	0.0013
5	0.0001	0.14	1.5×10^4	0.44	2.8×10^{-14}	1.86×10^8	0.58	0.42	0.0027

[a]Measured relative to ZrO_2-(1)-Zn-S (Φ_{uc} = 0.0023) via actinometry,[39] [b]$k_{TET} = 1/\tau_{s(bl)} - 1/\tau_s$, [c]$\Phi_{TET} = 1 - \tau_{s(bl)}/\tau_s$, [d]$J = \int_0^\infty F_A(\lambda)\varepsilon_S(\lambda)\lambda^4 d\lambda / \int_0^\infty F_A(\lambda)d\lambda$, [e]$k_{FRET} = 1/\tau_{A(bl)} - 1/\tau_A$, [f]$\Phi_{FRET} = 1 - \tau_{A(bl)}/\tau_A$, [g]$\Phi_{out} = 1 - \Phi_{FRET}$, [h]$\Phi_{TTA} = 2\Phi_{UC}/\Phi_{ISC}\Phi_{TET}\Phi_{FL}\Phi_{out}$.

neutron scattering experiments[76] and theoretical modelling[77] of molecular monolayers on metal oxide surfaces indicate that at high surface loadings, the molecular rotation and cross-surface mobility is significantly limited by steric hindrance due to tight intermolecular packing. Presumably this molecular motion is further hindered in the bilayer film because of the layered structure but further structural characterization is necessary to test this hypothesis.

3.4.1 ZrO_2-A-Zn-S TTA-UC Emission

Samples for emission measurements were prepared in a glove box under a N_2 atmosphere following a previously published procedure.[39] Upon 532 nm excitation (3 W/cm^2) all of the ZrO_2-**A**-Zn-**S** films exhibit a blue emission feature from 420-500 nm (Figure 5) that resembles emission from ZrO_2-**A** under direct excitation of **A** at 360 nm. This is in contrast to ZrO_2-**A** and ZrO_2-**S** under 532 nm excitation where no emission was observed in this region due to the lack of absorption and lower energy emission (λ_{em} = 670 nm), respectively. The sharp increase in intensity above 500 nm in Figure 5 can be attributed to scatter from the excitation source.

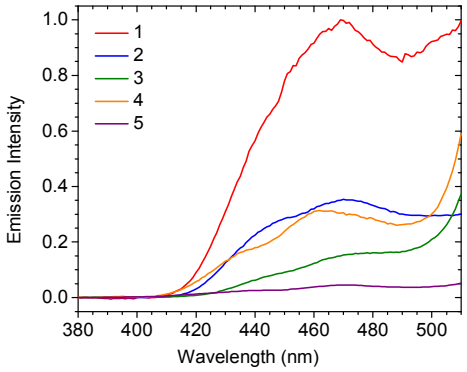

Figure 5. Emission spectra for ZrO_2-**A**-Zn-**S** in deaerated MeCN where **A** = **1**-**5** (λ_{ex} = 532 nm, 3 W/cm^2).

Upconverted emission quantum yields were measured relative to ZrO_2-**1**-Zn-**S** (Φ_{uc} = 0.0023)[39] and the results are summarized in Table 3. These measurements were performed under relatively high excitation intensities (3 W/cm^2) to ensure that all samples are operating in the maximum efficiency, linear regime (*vida infra*). The highest quantum yield was observed with our prototype bilayer, ZrO_2-**1**-Zn-**S**, and then decreases in the order **2** (0.0008) > **4** (0.0007) > **3** (0.0004) > **5** (0.0001).

The upconverted emission efficiency is equal to the products of the efficiency of each step in the TTA-UC process as shown in equation 1,[78]

$$\Phi_{UC} = \frac{\Phi_{ISC}\Phi_{FL}\Phi_{TET}\Phi_{out}\Phi_{TTA}}{2} \quad (1)$$

where Φ_{ISC} is the intersystem crossing yield of the sensitizer molecule, Φ_{FL} is the fluorescence quantum yield for **A**, Φ_{TET} is the sensitizer-to-acceptor triplet energy transfer yield, Φ_{out} is the fraction of upconverted states that generate photons that exit the sample and Φ_{TTA} is the efficiency of generating a singlet excited state *via* TTA. The two in the denominator is to account for the two photons in one photon out nature of the TTA-UC process. The measured and calculated quantum yield values for these events in the ZrO_2-**A**-Zn-**S** films are summarized in Table 3. Φ_{ISC} was not measured directly here but is assumed to be 1.0 as near unity intersystem crossing yields are known for platinum(II) porphyrin molecules.[78]

Sensitizer-to-acceptor triplet energy transfer rates and yields were determined using time-resolved spectroscopy following previous published procedures.[46] Briefly, phosphorescent emission lifetime from the sensitizer molecule (λ_{em} = 670 nm) was monitored following 532 nm excitation of two different samples, ZrO_2-**A**-Zn-**S** ($\tau_{s(bl)}$) and ZrO_2-**B**-Zn-**S** (τ_s). While the former samples exhibit porphyrin-to-anthracene TET, the latter contains terphenyl-4,4''-diylbisphosphonic acid (**B**) which retains the bilayer structure but is a photo- and electrochemically inert structural analogue of the acceptor molecule that does not undergo TET.[46, 79] The triplet energy transfer rate (k_{TET}) and yield (Φ_{TET}) were the calculated using equation 2 and 3

$$k_{TET} = \frac{1}{\tau_{s(bl)}} - \frac{1}{\tau_s} \quad (2)$$

$$\Phi_{TET} = 1 - \frac{\tau_{s(bl)}}{\tau_s} \quad (3)$$

and the results are summarized in Table 3.

The rate and efficiency of TET are primarily dictated by the thermodynamic driving-force for electron exchange and

View Article Online
DOI: 10.1039/C8CP03628D

the distance between the donor (**S**) and acceptor (**1-4**) molecules.[66] Of the acceptor molecules, **3** exhibited the fastest (k_{TET} = 2.1 × 10^4 s^{-1}) and most efficient (Φ_{TET} = 0.59) TET. This high yield is presumably due to the lack of phenyl or methyl groups between the anthracene core and the phosphonate metal ion binding group, effectively decreasing the distance between **S** and **3**. Based on the experimentally determined singlet excited state energies, one could assume that the triplet of **3** is also lower than the other complexes, and thus increases the driving force for TET, however we were unable to quantify the triplet energy by directly observing phosphorescent emission from **3**, or any of the acceptor molecules reported here, even at low temperatures and in the presence of methyl iodide.[80]

Interestingly, **1** and **2** exhibit the same TET rates (k_{TET} = 1.3 × 10^4 s^{-1}) and efficiencies (Φ_{TET} = 0.33). Given the difference in position of the surface/metal ion binding groups, one would anticipate differences in orientation and/or distance between **S** and **1** or **2** in the bilayer film. However, the similarity in TET rate/yield suggests that energetics, which are similar for the two molecules, is primarily responsible for dictating TET. Likewise, the methyl phosphonate complexes **4** and **5** exhibit similar TET metrics.

As noted above, Φ_{out} is the fraction of upconverted states that generate a photon that exit the sample. That is, photons that are not lost through quenching via **A**-to-**S** Förster resonance energy transfer (FRET).[81] Similar to the method described above for TET, FRET was quantified by measuring time-resolved emission at 470 nm upon direct excitation of **A** in films with, ZrO_2-**A**-Zn-**S** ($\tau_{A(bl)}$), and without, ZrO_2-**A** (τ_A), sensitizer which in this case quenches **A** emission. The FRET rate (k_{FRET}) and efficiency (Φ_{FRET}) were calculated using equation 4 and 5

$$k_{FRET} = \frac{1}{\tau_{A(S)}} - \frac{1}{\tau_A} \quad (4)$$

$$\Phi_{FRET} = 1 - \frac{\tau_{A(S)}}{\tau_A} \quad (5)$$

and the results are summarized in Table 3.

The rate of FRET is dictated by the **A** and **S** dipole orientations, spectral overlap between **A** emission and **S** absorption (J), and the distance between **A** and **S**.[82, 83]

J value were calculated and the result can be seen in Table 3. Compounds **1** and **2** have similar J values of 2.6×10^{-11} cm^3M^{-1} and 2.8×10^{-11} cm^3M^{-1}, respectively. Again, although we anticipate differences in orientation and distance between donor and acceptor in ZrO_2-**1**-Zn-**S** and ZrO_2-**2**-Zn-**S** films, the J values, combined with the similarity in k_{FRET} and Φ_{FRET}, indicate

that the differences in structure these two bilayers play a nominal role in dictating FRET.

In contrast, compound **3** has a similar J value as **4** (3.3×10^{-11} cm^3M^{-1} and 3.4×10^{-11} cm^3M^{-1}, respectively), but exhibits an order of magnitude faster FRET (k_{FRET} = 2.4 × 10^8 s^{-1}) and a more than two-fold higher FRET efficiency (Φ_{FRET} = 0.38). As was used to rationalize differences in TET, the distance between **S** and **3** is presumably decreased relative to the other **A** molecules resulting in an increased rate and efficiency of FRET in ZrO_2-**3**-Zn-**S**.

Interestingly, compound **5** exhibits the fastest (k_{FRET} = 1.86 × 10^8 s^{-1}) and most efficient (Φ_{FRET} = 0.58) FRET despite the three orders of magnitude lower J value (2.8 × 10^{-14} cm^3M^{-1}) relative to **1-4.** Collectively these results suggest that both structural factors and spectral overlap can play a critical role in dictating energy transfer in the bilayer. Presumably, molecular engineering could be used to maximize TET but minimize losses due to FRET. Unfortunately, we have no direct structural information about the interface. Efforts are currently underway to use DFT and dynamic molecular mechanics simulations to understand the role of the average intermolecular distance and orientation in dictating FRET and TET. Assuming that FRET is the dominant mechanism quenching the singlet excited state of **A**, then a Φ_{out} can be calculated using Φ_{out} = 1- Φ_{FRET}.

Using equation 1 and the values reported above,[78] the efficiency of triplet-triplet annihilation (Φ_{TTA}), was calculated and the values are reported in Table 3. The Φ_{TTA} decreases in the order **1** (0.0057) > **5** (0.0027) > **2** (0.0020) > **4** (0.0013) > **3** (0.0009). Of the various steps responsible for TTA-UC, these relatively low numbers suggest that Φ_{UC} in the bilayer films are primarily limited by the Φ_{TTA} value.

For ZrO_2-**1**-Zn-**S**, despite having the lowest Φ_{TET}, a combination of large Φ_{FL}, Φ_{out}, and Φ_{TTA} results in the highest overall UC yield. In terms of the efficiency of each process, molecules **1** and **2** are comparable except that the Φ_{TTA} of **2** (Φ_{TTA} = 0.0020) is ~3 times lower than for **1** (Φ_{TTA} = 0.0057) which is directly responsible for its lower Φ_{UC}. Interestingly this observation suggests that while the difference in structure between **1** and **2** has no bearing on TET or FRET, it does impact the cross surface migration and TTA events that are responsible for Φ_{TTA}.

While Φ_{TTA} is larger in **5** than for **2**-**4**, the drastically lower Φ_{FL} and Φ_{out} result in the significantly lower overall emission from the upconverted state of **5**. However, it is worth noting that in an integrated bilayer TTA-UC solar cell, electron injection from the UC state is typically much faster (~10^{12} s^{-1})[46] than the k_r, k_{nr}, or k_{FRET} values reported here (~10^8 s^{-1}) and may not be affected by Φ_{FL} and Φ_{out}. As such we anticipate an increased photocurrent from **5** relatives to **2**-**4**. Such an observation would emphasize the importance of molecular design in targeting specific applications of TTA-UC. Device measurements for TiO_2-**A**-Zn-**S** bilayers containing **1**-**5** are currently underway and will be reported at a later time.

3.4.2 TTA-UC Intensity Dependence

The emission intensity for ZrO_2-**A**-Zn-**S** films with respect to 532 nm excitation intensity are shown in Figure 6.[84, 85] All five bilayers exhibited a quadratic (slope = 2) to linear (slope = 1) intensity dependence that is symptomatic of a TTA-UC

View Article Online
DOI: 10.1039/C8CP03628D
Journal Name ARTICLE

mechanism.[85] The quadratic to linear crossover intensities, also known as the I_{th} value,[84] for ZrO_2-**A**-Zn-**S** decrease in the order **3** (880 mW/cm^2) ≈ **4** (870 mW/cm^2) > **2** (790 mW/cm^2) > **5** (750 mW/cm^2) > **1** (470 mW/cm^2).

The I_{th} value is inversely related to a several parameters as described in equation 6:

$$I_{th} = \frac{1}{\Phi_{TET} * \alpha(E) * (\tau_A^3)^2 * \gamma_{TTA}} \quad (6)$$

where τ_A^3 is the triplet excited state lifetime of **A**, Φ_{TET} is the TET efficiency, $\alpha(E)$ is the sensitizer absorption cross-section at 532 nm, and γ_{TTA} is the second-order rate constant for TTA.[46]

Following a previously published procedure,[86] τ_A^3 was determined for each **A**, using $\tau_A^3 = 2 \times \tau_{UC}$, where τ_{UC} is obtained by tail fitting the TTA-UC emission decay at 430 nm for a DMSO solution of **A** and **S** after 532 nm excitation. As can be seen in table 3 molecules **2**-**4** exhibit similar triplet excited state lifetimes on the order of 0.5 ms. In contrast, molecule **5** has the shortest lifetime of 0.07 ms which is in reasonable agreement with its singlet excited state behavior where it has an order of magnitude larger k_{nr} than the other molecules. Similar non-radiative decay channels may be accessible from the triplet state.

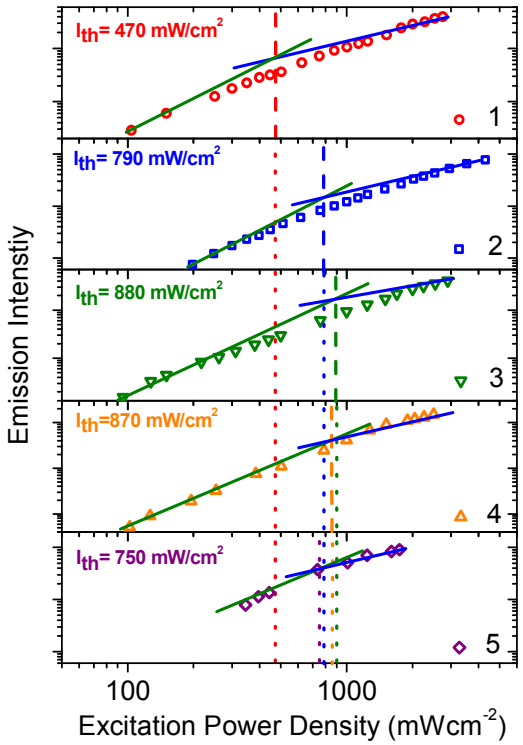

Figure 6. Emission intensity versus 532 nm excitation intensity for ZrO_2-**A**-Zn-**S** in MeCN where A = **1**-**5** (slopes of 1 and 2 are denoted by blue and green lines, respectively).

Strikingly, **1** has a τ_A^3 that is four times larger than **2**-**5**. This is particularly remarkable given that **1** and **2** give almost identical singlet excited state energetics and kinetics. It is possible that while the position of the phosphonate group has minimal influence on the singlet manifold, they may perturb the triplet state potential energy surface and subsequent mixing/overlapping between states as previously observed by Gray et al.[25]

Using equation 6, and the parameters listed in Table 4, γ_{TTA} was calculated for each **A**. The γ_{TTA} for ZrO_2-**A**-Zn-**S** ranges from 4.4 × 10^{-13} cm^{3}s^{-13} to 1 × 10^{-15} cm^{3}s^{-1} for **5** and **1**, respectively. Despite **1** having the lowest γ_{TTA}, it has the lowest I_{th} value due to the four-fold larger τ_A^3 ,whose exponent of 2 in equation 6, makes it a more strongly impactful variable in dictating I_{th} than γ_{TTA}. For **5**, the short lifetime is partially offset by the much larger γ_{TTA}, resulting in the second lowest I_{th} value of the series. If one were able to combine the γ_{TTA} of **5** while still retaining the long triplet excited state lifetime of **1**, I_{th} values on the order of solar flux (~5 mW/cm^2) would be feasible for TTA-UC emission from the bilayer film.

Table 4. I_{th} value, effective triplet-triplet interaction distance (a_0), acceptor triplet lifetime (τ_A^3), the second-order rate constant for the TTA (γ_{TTA}) and triplet diffusion coefficient (D).

	I_{th} (mW/cm^2)	α(E) (cm^{-1})[a]	a_0 (Å)[b]	τ_A^3 (ms)[c]	γ_{TTA} (cm^{3}s^{-1})[d]	D (cm^{2}s^{-1})[e]
1	470	575	8.6	2.02	1.0 × 10^{-15}	4.6 × 10^{-10}
2	790	565	9.7	0.55	7.6 × 10^{-15}	3.1 × 10^{-9}
3	880	450	16.0	0.48	6.9 × 10^{-15}	1.7 × 10^{-9}
4	890	555	11.2	0.62	3.9 × 10^{-15}	1.4 × 10^{-9}
5	750	570	8.9	0.07	4.4 × 10^{-13}	2.0 × 10^{-7}

[a] $\alpha(E)=5700\times A_{PtP(532\ nm)}$ [b]Estimated as $d_{A\text{-}A}$, [c]$\tau_A^3 = 2x\tau_{UC}$ where τ_{UC} is from an exponential tail fit to the upconverted emission decay from **A** (1000 μM) and **S** (0.5 μM) in DMSO (λ_{ex}= 532 nm), [d]$\gamma_{TTA}=1/(\Phi_{TET}\alpha(E)\alpha(\tau_A^3)^2 I_{th})$, [e]$D= \gamma_{TTA}/(8\pi a_0)$.

The values for γ_{TTA} in Table 4 are orders of magnitude smaller than for anthracene molecules in solution or crystals.[41] This observation could imply one of two things, either diffusion (i.e. rate of triplet migration across the surface) or the rate of TTA after the triplets have encountered are significantly slower in the bilayer film than in other media. If we assume, as with most other TTA-UC schemes,[87-89] that the rate limiting process is triplet migration, then the triplet exciton diffusion constant (D) can be calculated using $\gamma_{TTA}= (8\pi D a_0)$[28,84] where a_0 is the effective triplet-triplet interaction distance which in this case is assumed to be the intermolecular packing distance on the surface $d_{A\text{-}A}$. For ZrO_2-**A**-Zn-**S**, D increases in the order **5** (2.0 × 10^{-7} cm^{2}s^{-1}) > **4** (1.4 × 10^{-9} cm^{2}s^{-1}) ≈ **3** (1.7 × 10^{-9} cm^{2}s^{-1}) > **2** (3.1 × 10^{-9} cm^{2}s^{-1}) > **1** (4.6 × 10^{-10} cm^{2}s^{-1}) again with **5** and **1** being the upper and lower extremes of this parameter.

The lowest diffusion rate is observed with the diphenyl derivatives **1** and **2**. Presumably the phenyl groups provide some form of hindrance or molecular rigidity that decreases

View Article Online
DOI: 10.1039/C8CP03628D

electronic coupling between adjacent molecules. The order of magnitude difference between **1** and **2** may be a manifestation of how the molecules orient relative to the surface and to adjacent molecules. The origin of the two order of magnitude higher D for **5** (2.0×10^{-7} cm^2s^{-1}) is currently unclear to us. One could envision that lower steric hindrance or the forced relative orientation dictated by the methyl groups at the 2,6- position would favour face-to-face stacking of the acceptor molecules. Alternatively, the flexibility afforded by the methyl phosphonate group may allow for additional mobility of the tethered molecule such that it can sample a larger orientation space on the timescales of triplet diffusion. These observations again emphasize the importance of obtaining either experimental or theoretical insights into the molecular structure at the interface. Understanding and then controlling these structural parameters is critical to improving TTA-UC efficiencies in self-assembled systems.

As a somewhat unrelated side note, it was intriguing to us that there is a strong linear correlation (R-sq = 0.98) between the I_{th} values and Φ_{TTA} for this series of molecules (Figure S7). To the best of our knowledge there is no intrinsic or causal reason for this correlation. The values are measured independently and Φ_{TTA} is effectively the y-offset of the intensity dependence graph (i.e. the I_{th} curve). We attempted to determine if this was a general trend among TTA-UC system's but unfortunately a majority the manuscripts that report Φ_{TTA} do not also include the I_{th} values, or vice versa, under the same conditions. It is however worth mentioning that if this linear relationship holds true, then increasing Φ_{TTA} to 0.01, for example, would result in an I_{th} value of 5 mW/cm^2.

Given its strong impact on both I_{th} and Φ_{UC}, these results indicate that dramatically increasing Φ_{TTA} is a necessary step in increasing the efficiency of TTA-UC in the bilayer films. One contribution to Φ_{TTA} is the probability of obtaining a singlet excited state after annihilation of two triplet states, sometimes denoted as f.[90] Pure spin statistics limit f to only 1/9 ($\Phi_{TTA(max)}$ = 0.11).[91] However this fraction can be increased if the quintet state is energetically inaccessible (Φ_{TTA} = 0.25), and even further so if an upconverted triplet state can undergo reverse ISC into the singlet state. Experimental f values as high as 0.66 have been reported.[92] Presumably, as is well known in singlet fission (SF), or roughly the reverse of TTA, molecular packing could have a profound influence on the rate and thus the efficiency of TTA. However, the role of relative molecular orientation, if any, in dictating f is currently unknown but newly developed self-assembled systems may provide a scaffolding to study this relationship.

4. Conclusion

Here we have reported the synthesis and photophysical characterization of phosphonated anthracene derivatives that act as the acceptor molecule in self-assembled bilayers for TTA-UC. The acceptor molecules are composed of an anthracene core functionalized with 9,10- or 2,6- phenyl, methyl, or directly bound phosphonic acid groups for metal ion coordination. In terms of ZrO_2 surface binding, the molecules obey Langmuir isotherm behavior with a maximum surface loading giving a center-to-center packing distance on the order of 10 Å. Binding the molecules to the surface has minimal influence on the photophysical properties of the dyes relative to solution. Increased steric hindrance at the 9,10-positions, as opposed to the 2,6-position, was found to increase the photostability of the dyes at the interface with the primary decomposition mechanism likely being a reaction with oxygen with the anthracene core.

The acceptor molecules were incorporated into self-assembled bilayer films with zinc as the linking ion and platinum porphyrin as the sensitizer. All five films facilitate green-to-blue photon upconversion with UC efficiencies as high as 0.0023 for **1**. Φ_{TTA} and not Φ_{TET}, Φ_{FL}, or Φ_{out}, was found to be the primary variable limiting the TTA-UC emission efficiency. Films containing compound **1** also exhibited the lowest I_{th} value despite having a lower second-order rate constant for TTA and diffusion constant. Regardless of having similar photophysical properties, variation in the position of the phosphonic acid on diphenylanthracene (**1** versus **2**) resulted in dramatically different Φ_{TTA}, I_{th} values, γ_{TTA}, and D. Molecule **5**, with a methylphosphoic group at the 2,6- position exhibited the highest triplet exciton diffusion rate and γ_{TTA} but they could not compensate for the short triplet lifetime and low fluorescence quantum yield and thus **5** exhibited the least efficient TTA-UC emission. Interestingly, we observed a strong linear correlation between Φ_{TTA} and the I_{th} value but the cause of this relationship, if any, is unclear.

Collectively the result reported here point to three primary conclusions, 1) increasing Φ_{TTA} is the key factor in lowering the I_{th} value and increasing Φ_{UC} in the bilayer film, 2) the structure of the molecule, and not simply the energetics, can be, but is not always, a critical factor influencing TTA-UC in the bilayer architecture, and 3) measuring and modelling the structure at these interfaces will be a necessary step in fully explaining and then controlling migration, triplet energy transfer, back energy transfer and ultimately the TTA-UC efficiency in self-assembled bilayer films.

5. Conflicts of interest

There are no conflicts to declare

6. Acknowledgements

View Article Online
DOI: 10.1039/C8CP03628D

This material is based upon work supported by the National Science Foundation under Grant No. DMR-1752782. Time-resolved emission measurements for TTA-UC were performed on a spectrometer supported by the National Science Foundation under Grant No. CHE-1531629.

7. Notes and references

1. J. Zhou, Q. Liu, W. Feng, Y. Sun and F. Li, *Chemical Reviews*, 2015, 115, 395-465.
2. B. S. M., L. Christoph and K. Ingo, *Advanced Functional Materials*, 2012, 22, 4360-4368.
3. H.-i. Kim, S. Weon, H. Kang, A. L. Hagstrom, O. S. Kwon, Y.-S. Lee, W. Choi and J.-H. Kim, *Environmental Science & Technology*, 2016, 50, 11184-11192.
4. Y. Y. Cheng, B. Fuckel, R. W. MacQueen, T. Khoury, R. G. C. R. Clady, T. F. Schulze, N. J. Ekins-Daukes, M. J. Crossley, B. Stannowski, K. Lips and T. W. Schmidt, *Energy & Environmental Science*, 2012, 5, 6953-6959.
5. S. P. Hill, T. Dilbeck, E. Baduell and K. Hanson, *ACS Energy Letters*, 2016, 1, 3-8.
6. T. Dilbeck, S. P. Hill and K. Hanson, *Journal of Materials Chemistry A*, 2017, 5, 11652-11660.
7. A. Nattestad, Y. Y. Cheng, R. W. MacQueen, T. F. Schulze, F. W. Thompson, A. J. Mozer, B. Fückel, T. Khoury, M. J. Crossley, K. Lips, G. G. Wallace and T. W. Schmidt, *The Journal of Physical Chemistry Letters*, 2013, 4, 2073-2078.
8. Y. L. Lin, M. Koch, A. N. Brigeman, D. M. E. Freeman, L. Zhao, H. Bronstein, N. C. Giebink, G. D. Scholes and B. P. Rand, *Energy & Environmental Science*, 2017, 10, 1465-1475.
9. T. F. Schulze, Y. Y. Cheng, B. Fückel, R. W. MacQueen, A. Danos, N. J. L. K. Davis, M. J. Y. Tayebjee, T. Khoury, R. G. C. R. Clady, N. J. Ekins-Daukes, M. J. Crossley, B. Stannowski, K. Lips and T. W. Schmidt, *Australian Journal of Chemistry*, 2012, 65, 480-485.
10. C. Simpson, T. M. Clarke, R. W. MacQueen, Y. Y. Cheng, A. J. Trevitt, A. J. Mozer, P. Wagner, T. W. Schmidt and A. Nattestad, *Physical Chemistry Chemical Physics*, 2015, 17, 24826-24830.
11. Y. Zhou, S. P. Hill and K. Hanson, 2017. *J. Photon. Energy 2018, 8, 022004*.
12. W. Shockley and H. J. Queisser, *Journal of Applied Physics*, 1961, 32, 510-519.
13. V. Gray, D. Dzebo, M. Abrahamsson, B. Albinsson and K. Moth-Poulsen, *Physical Chemistry Chemical Physics*, 2014, 16, 10345-10352.
14. N. J. Ekins-Daukes and T. W. Schmidt, *Applied Physics Letters*, 2008, 93, 063507.
15. T. N. Singh-Rachford and F. N. Castellano, *Coordination Chemistry Reviews*, 2010, 254, 2560-2573.
16. P. Duan, N. Yanai and N. Kimizuka, *Journal of the American Chemical Society*, 2013, 135, 19056-19059.
17. P. Duan, N. Yanai, H. Nagatomi and N. Kimizuka, *Journal of the American Chemical Society*, 2015, 137, 1887-1894.
18. P. C. Boutin, K. P. Ghiggino, T. L. Kelly and R. P. Steer, *The Journal of Physical Chemistry Letters*, 2013, 4, 4113-4118.
19. P. B. Merkel and J. P. Dinnocenzo, *Journal of Luminescence*, 2009, 129, 303-306.
20. M. Hosoyamada, N. Yanai, T. Ogawa and N. Kimizuka, *Chemistry – A European Journal*, 2016, 22, 2060-2067.
21. R. Vadrucci, C. Weder and Y. C. Simon, *Journal of Materials Chemistry C*, 2014, 2, 2837-2841.
22. R. S. Khnayzer, J. Blumhoff, J. A. Harrington, A. Haefele, F. Deng and F. N. Castellano, *Chemical Communications*, 2012, 48, 209-211.
23. V. Gray, D. Dzebo, A. Lundin, J. Alborzpour, M. Abrahamsson, B. Albinsson and K. Moth-Poulsen, *Journal of Materials Chemistry C*, 2015, 3, 11111-11121.
24. F. Zhong and J. Zhao, *Dyes and Pigments*, 2017, 136, 909-918.
25. V. Gray, A. Dreos, P. Erhart, B. Albinsson, K. Moth-Poulsen and M. Abrahamsson, *Physical Chemistry Chemical Physics*, 2017, 19, 10931-10939.
26. V. Gray, K. Moth-Poulsen, B. Albinsson and M. Abrahamsson, *Coordination Chemistry Reviews*, 2018, 362, 54-71.
27. N. Kimizuka, N. Yanai and M.-a. Morikawa, *Langmuir*, 2016, 32, 12304-12322.
28. T. Ogawa, N. Yanai, A. Monguzzi and N. Kimizuka, *Scientific Reports*, 2015, 5, 10882.
29. V. Gray, K. Börjesson, D. Dzebo, M. Abrahamsson, B. Albinsson and K. Moth-Poulsen, *The Journal of Physical Chemistry C*, 2016, 120, 19018-19026.
30. V. Gray, B. Kucukoz, F. Edhborg, M. Abrahamsson, K. Moth-Poulsen and B. Albinsson, *Physical Chemistry Chemical Physics*, 2018, 20, 7549-7558.
31. C. Fan, W. Wu, J. J. Chruma, J. Zhao and C. Yang, *Journal of the American Chemical Society*, 2016, 138, 15405-15412.
32. I. Keita, M. Masa‐aki, C. Chie, Y. Teppei, I. Katsunori, K. Mika and K. Nobuo, *Angewandte Chemie International Edition*, 2015, 54, 1532-1536.
33. S. Ahmad, J. Liu, C. Gong, J. Zhao and L. Sun, *ACS Applied Energy Materials*, 2018, 1, 249-253.
34. J. Park, M. Xu, F. Li and H.-C. Zhou, *Journal of the American Chemical Society*, 2018, 140, 5493-5499.
35. J. S. Lissau, J. M. Gardner and A. Morandeira, *The Journal of Physical Chemistry C*, 2011, 115, 23226-23232.
36. J. S. Lissau, D. Nauroozi, M.-P. Santoni, S. Ott, J. M. Gardner and A. Morandeira, *The Journal of Physical Chemistry C*, 2015, 119, 25792-25806.
37. J. S. Lissau, D. Nauroozi, M.-P. Santoni, T. Edvinsson, S. Ott, J. M. Gardner and A. Morandeira, *The Journal of Physical Chemistry C*, 2015, 119, 4550-4564.
38. J. S. Lissau, D. Nauroozi, M.-P. Santoni, S. Ott, J. M. Gardner and A. Morandeira, *The Journal of Physical Chemistry C*, 2013, 117, 14493-14501.
39. S. P. Hill, T. Banerjee, T. Dilbeck and K. Hanson, *The Journal of Physical Chemistry Letters*, 2015, 6, 4510-4517.
40. S. P. Hill and K. Hanson, *Journal of the American Chemical Society*, 2017, 139, 10988-10991.
41. L. Frazer, J. K. Gallaher and T. W. Schmidt, *ACS Energy Letters*, 2017, 2, 1346-1354.
42. H. Kenneth, T. D. A., V. A. K., B. M. Kyle, L. Hanlin, A. Leila, S. Wenjing, A. D. L., N. M. R., G. C. R. K., C. J. J. and M. T. J., *Angewandte Chemie International Edition*, 2012, 51, 12782-12785.

View Article Online
DOI: 10.1039/C8CP03628D

43. O. O. Ogunsolu, I. A. Murphy, J. C. Wang, A. Das and K. Hanson, *ACS Applied Materials & Interfaces*, 2016, 8, 28633-28640.
44. W. Song, C. R. K. Glasson, H. Luo, K. Hanson, M. K. Brennaman, J. J. Concepcion and T. J. Meyer, *The Journal of Physical Chemistry Letters*, 2011, 2, 1808-1813.
45. S.-H. A. Lee, N. M. Abrams, P. G. Hoertz, G. D. Barber, L. I. Halaoui and T. E. Mallouk, *The Journal of Physical Chemistry B*, 2008, 112, 14415-14421.
46. T. Dilbeck, J. C. Wang, Y. Zhou, A. Olsson, M. Sykora and K. Hanson, *The Journal of Physical Chemistry C*, 2017, DOI: 10.1021/acs.jpcc.7b07003.
47. O. O. Ogunsolu, J. C. Wang and K. Hanson, *ACS Applied Materials & Interfaces*, 2015, 7, 27730-27734.
48. B. Tyagi, K. Sidhpuria, B. Shaik and R. V. Jasra, *Industrial & Engineering Chemistry Research*, 2006, 45, 8643-8650.
49. J. V. Morris, M. A. Mahaney and J. R. Huber, *The Journal of Physical Chemistry*, 1976, 80, 969-974.
50. M. I. Aralaguppi, C. V. Jadar and T. M. Aminabhavi, *Journal of Chemical & Engineering Data*, 1999, 44, 216-221.
51. J. G. Baragi, M. I. Aralaguppi, T. M. Aminabhavi, M. Y. Kariduraganavar and A. S. Kittur, *Journal of Chemical & Engineering Data*, 2005, 50, 910-916.
52. M. Pramanik, N. Chatterjee, S. Das, K. D. Saha and A. Bhaumik, *Chemical Communications*, 2013, 49, 9461-9463.
53. Z. Jibo, X. Bin, C. Jinlong, M. Suqian, D. Yujie, W. Lijuan, L. Bao, Y. Ling and T. Wenjing, *Advanced Materials*, 2014, 26, 739-745.
54. T. M. Balthazor and R. C. Grabiak, *The Journal of Organic Chemistry*, 1980, 45, 5425-5426.
55. Y. Gong, Y. Zhou, J. Qin, J. Li and R. Cao, *Journal of Molecular Structure*, 2010, 963, 76-81.
56. X. X. Wang, Jun; Chen, Ning; Wang, Xiaoqing; Yang, Wenjun, *Qingdao Keji Daxue Xuebao, Ziran Kexueban*, 2008, 29, 1-4.
57. S. Duan, J. Turk, J. Speigle, J. Corbin, J. Masnovi and R. J. Baker, *The Journal of Organic Chemistry*, 2000, 65, 3005-3009.
58. A. L. J. Beckwith and W. A. Waters, *J Chem Soc*, 1956, DOI: DOI 10.1039/jr9560001108, 1108-1115.
59. R. N. Jones, *Chemical Reviews*, 1947, 41, 353-371.
60. K. Terada, K. Kobayashi, J. Hikita and M.-a. Haga, *Chemistry Letters*, 2009, 38, 416-417.
61. M.-a. Haga, K. Kobayashi and K. Terada, *Coordination Chemistry Reviews*, 2007, 251, 2688-2701.
62. Y. Tachibana, J. E. Moser, M. Grätzel, D. R. Klug and J. R. Durrant, *The Journal of Physical Chemistry*, 1996, 100, 20056-20062.
63. M. A. Butler and D. S. Ginley, *J Electrochem Soc*, 1978, 125, 228-232.
64. I. Langmuir, *Journal of the American Chemical Society*, 1916, 38, 2221-2295.
65. L. A. Gallagher, S. A. Serron, X. Wen, B. J. Hornstein, D. M. Dattelbaum, J. R. Schoonover and T. J. Meyer, *Inorganic Chemistry*, 2005, 44, 2089-2097.
66. D. L. Dexter, *The Journal of Chemical Physics*, 1953, 21, 836-850.
67. H. Sternlicht, G. C. Nieman and G. W. Robinson, *The Journal of Chemical Physics*, 1963, 38, 1326-1335.
68. T. Azumi and S. P. McGlynn, *The Journal of Chemical Physics*, 1963, 39, 1186-1194.
69. I. R. R. and C. F. N., *Angewandte Chemie International Edition*, 2006, 45, 5957-5959.
70. L. Slavětínská, J. Mosinger and P. Kubát, *Journal of Photochemistry and Photobiology A: Chemistry*, 2008, 195, 1-9.
71. K. Hanson, M. K. Brennaman, H. Luo, C. R. K. Glasson, J. J. Concepcion, W. Song and T. J. Meyer, *ACS Applied Materials & Interfaces*, 2012, 4, 1462-1469.
72. R. Castro-Olivares, G. Günther, A. L. Zanocco and E. Lemp, *Journal of Photochemistry and Photobiology A: Chemistry*, 2009, 207, 160-166.
73. J. C. Wang, K. Violette, O. O. Ogunsolu, S. Cekli, E. Lambers, H. M. Fares and K. Hanson, *Langmuir*, 2017, DOI: 10.1021/acs.langmuir.7b01964.
74. W. Gao, L. Dickinson, C. Grozinger, F. G. Morin and L. Reven, *Langmuir*, 1996, 12, 6429-6435.
75. B. L. Frey, D. G. Hanken and R. M. Corn, *Langmuir*, 1993, 9, 1815-1820.
76. V. Vaissier, V. G. Sakai, X. Li, J. T. Cabral, J. Nelson and P. R. F. Barnes, *Scientific Reports*, 2016, 6, 39253.
77. V. Vaissier and T. Van Voorhis, *The Journal of Physical Chemistry C*, 2017, 121, 12562-12568.
78. T. W. Schmidt and F. N. Castellano, *The Journal of Physical Chemistry Letters*, 2014, 5, 4062-4072.
79. J. C. Wang, I. A. Murphy and K. Hanson, *The Journal of Physical Chemistry C*, 2015, 119, 3502-3508.
80. A. P. Marchetti and D. R. Kearns, *Journal of the American Chemical Society*, 1967, 89, 768-777.
81. G. L., A. K. A., N. V. and M. B. G., *Angewandte Chemie*, 2001, 113, 3733-3736.
82. C. A. R., M. I. L. and M. Hedi, *ChemPhysChem*, 2006, 7, 47-57.
83. J. R. Lakowicz, MyiLibrary. and SpringerLink (Online service), Springer,, New York, 3rd edn., 2006, pp. 1 online resource (xxvi, 954 p.).
84. A. Monguzzi, J. Mezyk, F. Scotognella, R. Tubino and F. Meinardi, *Physical Review B*, 2008, 78, 195112.
85. A. Haefele, J. Blumhoff, R. S. Khnayzer and F. N. Castellano, *The Journal of Physical Chemistry Letters*, 2012, 3, 299-303.
86. X. Li and M. L. Tang, *Chemical Communications*, 2017, 53, 4429-4440.
87. E. N. Bodunov, M. N. Berberan-Santos and J. M. G. Martinho, *Chemical Physics*, 2005, 316, 217-224.
88. D. Dzebo, K. Börjesson, V. Gray, K. Moth-Poulsen and B. Albinsson, *The Journal of Physical Chemistry C*, 2016, 120, 23397-23406.
89. T. N. Singh-Rachford and F. N. Castellano, *The Journal of Physical Chemistry A*, 2009, 113, 5912-5917.
90. A. Monguzzi, R. Tubino, S. Hoseinkhani, M. Campione and F. Meinardi, *Physical Chemistry Chemical Physics*, 2012, 14, 4322-4332.
91. J. Saltiel, G. R. March, W. K. Smothers, S. A. Stout and J. L. Charlton, *Journal of the American Chemical Society*, 1981, 103, 7159-7164.
92. Y. Y. Cheng, T. Khoury, R. G. C. R. Clady, M. J. Y. Tayebjee, N. J. Ekins-Daukes, M. J. Crossley and T. W. Schmidt, *Physical Chemistry Chemical Physics*, 2010, 12, 66-71.

View Article Online
DOI: 10.1039/C8CP03628D

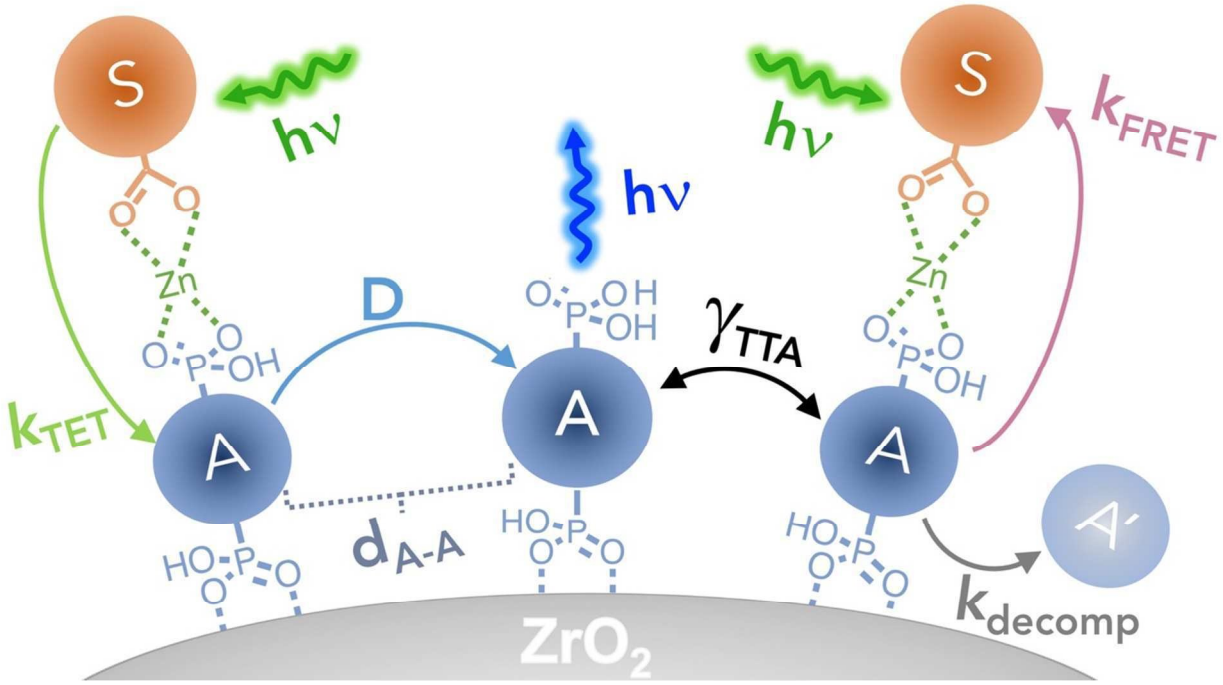

This report provides insights into the TTA-UC process with respect to the structure of the acceptor molecule in self-assembled bilayer films.